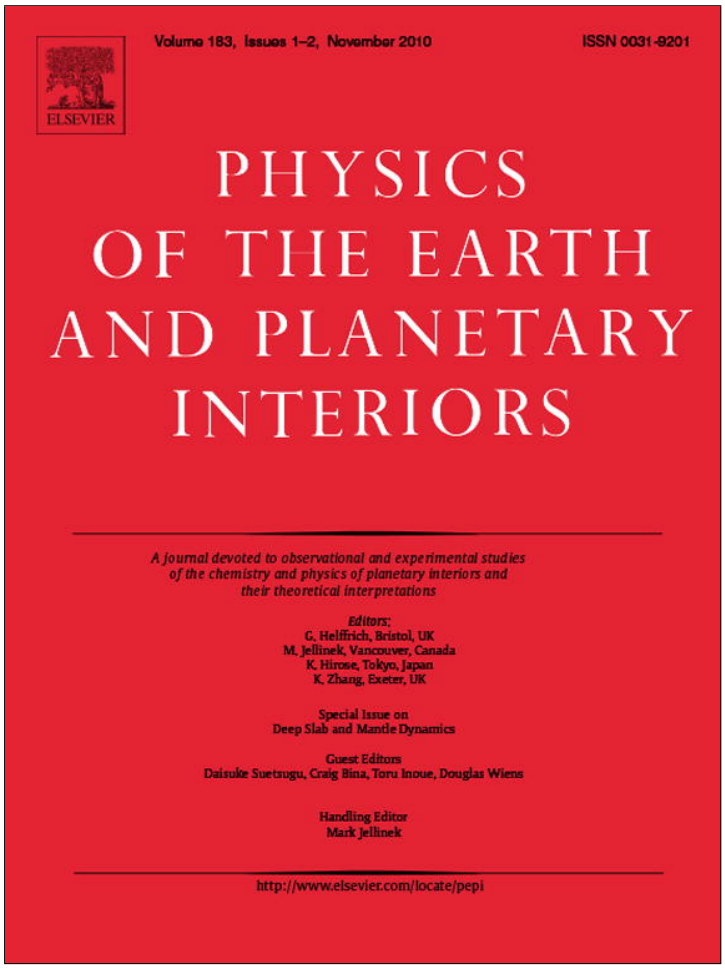

Physics of the Earth and Planetary Interiors 183 (2010) 33–43

Contents lists available at ScienceDirect

Physics of the Earth and Planetary Interiors

journal homepage: www.elsevier.com/locate/pepi

Anisotropic structures of the upper mantle beneath the northern Philippine Sea region from Rayleigh and Love wave tomography

Takehi Isse[a,*], Hajime Shiobara[a], J.-P. Montagner[b], Hiroko Sugioka[c], Aki Ito[c], Azusa Shito[c], Toshihiko Kanazawa[a], Kazunori Yoshizawa[d]

[a] Earthquake Research Institute, University of Tokyo, 1-1-1, Yayoi, Bunkyo-ku, Tokyo 113-0032, Japan
[b] Department of Seismology, Institut de Physique du Globe de Paris, 4 Place Jussieu, Case 89, 75005 Paris, France
[c] Institute for Research on Earth Evolution (IFREE), Japan Agency for Marine-Earth Science and Technology (JAMSTEC), Yokosuka 237-0061, Japan
[d] Earth and Planetary Dynamics, Faculty of Science, Hokkaido University, Sapporo 060-0810, Japan

ARTICLE INFO

Article history:
Received 7 September 2009
Received in revised form 26 March 2010
Accepted 16 April 2010

Guest Editors
Daisuke Suetsugu
Craig Bina
Toru Inoue
Douglas Wiens

Editor
Mark Jellinek

Keywords:
Surface wave tomography
Anisotropy
Ocean bottom seismometer
Upper mantle structure
Philippine Sea

ABSTRACT

Seismic anisotropy can provide fundamental information on past and present-day deformation processes in the upper mantle. Using Rayleigh and Love waves recorded by land and seafloor broadband seismometers, we analyzed the isotropic and anisotropic shear-wave velocity structures in the northern Philippine Sea region. We found that the fast directions of azimuthal anisotropy are parallel to the directions of ancient seafloor spreading in the lithosphere of the Shikoku and West Philippine Basins and Pacific Ocean, whereas they are parallel to the direction of the present-day absolute plate motion (APM) in the asthenosphere of the Shikoku Basin, and oblique to the direction of the APM in the Pacific Ocean (by ~30°) and in the northern part of the West Philippine Basin (by ~55°). In the subduction zones around the Philippine Sea plate, the fast direction of azimuthal anisotropy is trench-parallel in the Ryukyu arc, and oriented NW–SE in the Izu–Ogasawara island arc. The Philippine Sea plate, which is a single plate, shows very large lateral variations in azimuthal and radial anisotropies compared with the Pacific plate.

1. Introduction

The Philippine Sea, located in the northwestern part of the Pacific Ocean, consists of several small basins, ridges and troughs with various seafloor ages (Fig. 1(a)). The age of the seafloor in the West Philippine Basin is 35–50 Ma (Taylor and Goodliffe, 2004), whereas that in the Shikoku Basin and the Parece-Vela Basin is 15–30 Ma (Okino et al., 1999). Seafloor spreading within the Mariana Trough started at about 6 Ma (Hussong and Uyeda, 1981). These ages have been explained in terms of two episodes of back-arc spreading (e.g., Hall et al., 1995). The older parts of the Pacific plate (seafloor ages of around 150 Ma) are subducting beneath the Philippine Sea plate along the Izu–Bonin(Ogasawara)–Mariana island arc at the eastern boundary of the Philippine Sea plate. The northern margin of the Philippine Sea plate is subducting beneath the Eurasian plate.

The upper mantle structure beneath the Philippine Sea plate, which may reflect the complex evolutionary history described above, as well as lateral variations caused by modern-day subduction, has been extensively studied using surface waves (e.g., Kanamori and Abe, 1968; Oda and Senna, 1994; Lebedev et al., 1997; Nakamura and Shibutani, 1998) and P- and S-wave travel times (Gorbatov and Kennett, 2003). However, a lack of both seismic stations and earthquakes in the central Philippine Sea has limited the spatial resolution of the upper mantle in this region in all previous models, especially in the southern part of the Philippine Sea, making it difficult to reduce artifacts caused by structures located outside the Philippine Sea.

Isse et al. (2006) produced an enhanced-resolution 3-D shear-wave speed structure in the upper mantle beneath the Philippine Sea and the surrounding region from Rayleigh waves recorded by land-based and long-term broadband ocean bottom seismographic stations. This model showed a strong correlation between the shear-wave speed structure in the upper 120 km and the age of the province, and fast anomalies of the subducted slab of the Pacific plate (Isse et al., 2006). Although the spatial resolution was

* Corresponding author.
E-mail address: tisse@eri.u-tokyo.ac.jp (T. Isse).

0031-9201/$ – see front matter © 2010 Elsevier B.V. All rights reserved.
doi:10.1016/j.pepi.2010.04.006

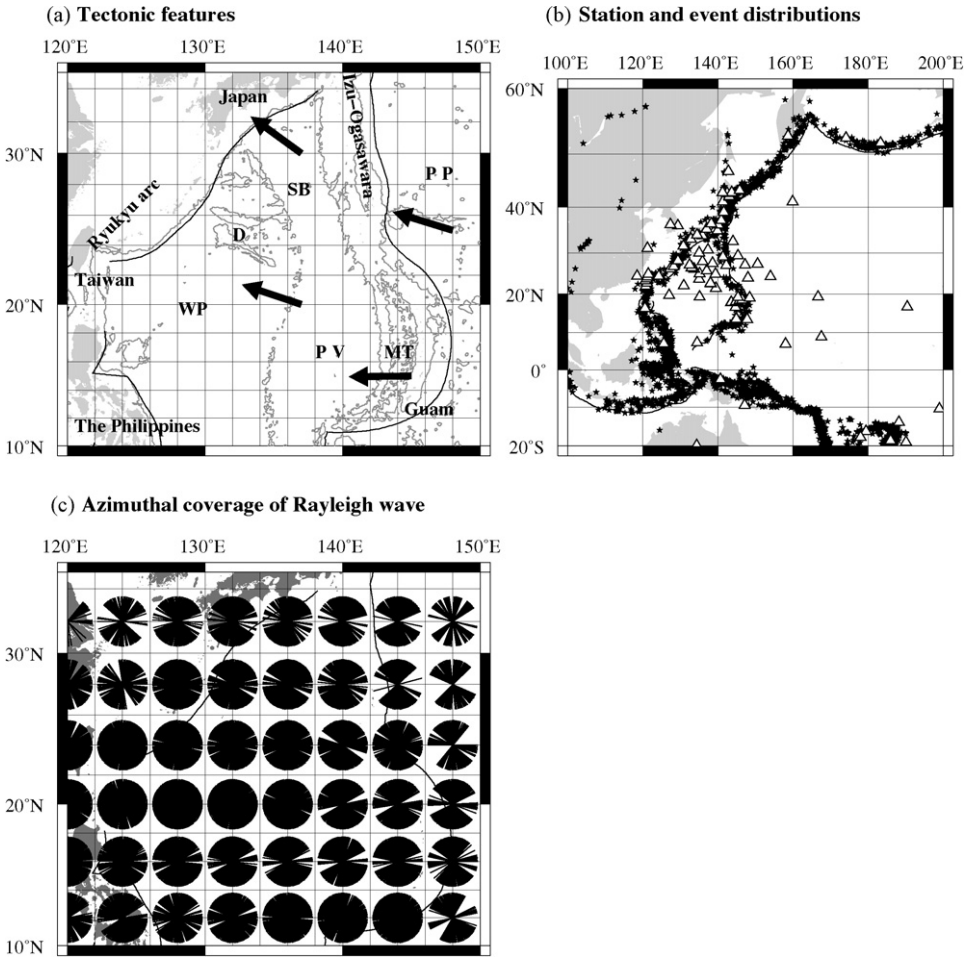

Fig. 1. (a) Tectonic features of the Philippine Sea region. Grey contour indicates bathymetry at a depth of 3500 m. Black lines indicate the boundary of the Philippine Sea plate. Letters represent marginal basins and tectonic features, as follows: D, Amami Plateau, and Daito and Oki-Daito ridges; MT, Mariana Trough; PP, Pacific plate; PV, Parece-Vela Basin; SB, Shikoku Basin; WP, West Philippine Basin. Arrows indicate the direction of the present-day absolute plate motion based on the NNR-NUVEL1A model (DeMets et al., 1994). (b) Geographical distributions of events (stars) and stations (triangles) used in this study. Black lines represent plate boundaries. (c) Geographical distribution of the azimuthal path coverage of Rayleigh waves used in this study in $4^\circ \times 4^\circ$ blocks. The azimuths of rays passing through each block are plotted at the centre of the block. Azimuthal coverage is very good in the northern part of the Philippine Sea.

improved by using newly developed broadband ocean bottom seismometers (BBOBSs) (Kanazawa et al., 2001; Shiobara et al., 2001), it is insufficient to resolve fine-scale differences within the region (Isse et al., 2006). This limitation arises in part because BBOBS data make up only about 10% of the total data set.

In 2005–2008, a new, dense array of seafloor observation stations was deployed in the Philippine Sea as part of the Stagnant Slab Project (SSP), with the aim of investigating the stagnant slab in more detail based on geophysical observations, high-pressure experiments, and computer simulations (Shiobara et al., 2009). Geophysical observations on the seafloor in the Philippine Sea, using BBOBSs and ocean bottom electro-magnetometers (OBEMs), were conducted in three phases, each consisting of a 1-year deployment using 12–16 BBOBSs and 11–14 OBEMs, resulting in a 3-year time series of data.

Using all Rayleigh wave observations from land stations around the Philippine Sea, the first two phases of experiments by SSP, and earlier deployments of BBOBSs in the Philippine Sea region, Isse et al. (2009) constructed a new 3-D model of the isotropic shear-wave structure of the upper mantle in and around the Philippine Sea region, attaining the highest resolution ever obtained from surface waves. The authors have detected three separate slow anomalies with widths of about 500 km in the mantle wedge at depths shallower than 100 km beneath the Izu–Bonin–Mariana island arc. These three anomalies have a close relationship with three groups of frontal and rear arc volcanoes characterized by distinct Sr, Nd, and Pb isotope ratios. The authors suggested that each anomaly is the site of large-scale flow of upper mantle into the mantle wedge, and that each contains a component from the adjacent subducting slab (Isse et al., 2009). This model was based on 2.5–8 times more data than that considered by Isse et al. (2006), as well as 5–13 times the amount of the BBOBSs and a wider spatial distribution of BBOBSs, thereby resulting in a higher-resolution model than that proposed by Isse et al. (2006).

Isotropic heterogeneous structures are interpreted as thermal and/or compositional heterogeneity within the upper mantle, whereas seismic anisotropy is related to the on-going deformation processes and is usually interpreted in terms of the flow pattern in the upper mantle (e.g., Montagner and Tanimoto, 1991). Therefore, it is important to study anisotropic structures of the upper mantle to reveal dynamic processes occurring in this zone.

It has been widely established that the Earth's upper mantle is anisotropic. For example, seismic anisotropy has been observed in a variety of forms, such as the azimuthal variation of Pn velocities in oceans (Hess, 1964), S-wave splitting in teleseismic SKS waves (Vinnik et al., 1989), the discrepancy between Rayleigh and Love wave dispersions (Aki and Kaminuma, 1963), and azimuthal variations in surface wave velocities (Forsyth, 1975).

The main cause of upper mantle anisotropy is the alignment (lattice preferred orientation, LPO) of anisotropic crystals induced by convective flow (Nicolas and Christensen, 1987). The occurrence of horizontal, melt-rich layers embedded in the upper mantle (shape preferred orientation, SPO) is another cause of radial anisotropy in the upper mantle (Kawakatsu et al., 2009). It is usually assumed that the fast axis of olivine is aligned with the flow direction.

Important evidence regarding anisotropy in oceanic plates can be derived from surface waves. The distribution of azimuthal anisotropy confirms the correlation between present-day or fossil directions of plate motion and the direction of maximum anisotropy in the uppermost mantle (Nishimura and Forsyth, 1989; Montagner, 2002; Debayle et al., 2005). Radial anisotropy, observed as the discrepancy between Rayleigh and Love wave dispersions, has also been derived on a global scale (Montagner and Tanimoto, 1991; Ekström and Dziewonski, 1998). In the present study, we analyze the azimuthal and radial anisotropic structures of the northern Philippine Sea region and show their relationships with plate motion and deformation processes using the phase-velocity dispersion curves of Love and Rayleigh waves.

2. Data and method

2.1. Dataset

We analyzed broadband seismograms collected by F-net, the OHP network, the SPANET network and the IRIS network, as well as temporary seafloor observations by BBOBSs at 20°S–60°N, 100°E–160°W (Fig. 1(b)).

We analyzed 4179 events (Mb or Mw > 5.5) that occurred in the above region since 1990. Compared to the previous models (Isse et al., 2006, 2009), a larger area is considered in the present case, the numbers of events and stations are increased to improve the azimuthal coverage in the Philippine Sea region, and we added seismograms obtained during the third phase of BBOBS observations in 2007–2008, as part of SSP. Isse et al. (2006) used 31 land stations and 20 BBOBS stations, while Isse et al. (2009) used 37 land and 37 BBOBS stations. In the present study, we used 58 land stations and 38 BBOBS stations. Fig. 1(c) shows the azimuthal coverage of the Rayleigh waves used in this study in each $4^\circ \times 4^\circ$ blocks. The azimuthal coverage is very good over most of the Philippine Sea region, especially in the northern part, whereas it is slightly degraded in the Pacific Ocean.

Fig. 2 shows the vertical and transverse components of displacement waveforms recorded by BBOBSs and two land stations band-pass filtered from 10 to 167 s and from instrumental responses are removed. P, S, and Rayleigh waves are evident in the vertical component of all BBOBSs and land stations. Love waves are evident in the transverse component of both BBOBSs and land stations, although BBOBS data are noisier than data from land stations. Some BBOBS seismograms (e.g., T11), are of high quality and are comparable with those recorded by land stations. The signal-to-noise ratios of the vertical components of all BBOBS data and of the transverse components of some BBOBS data are comparable with those of land stations.

2.2. Measurement of path-averaged phase speed of Rayleigh and Love waves

We measured the phase speed of the fundamental mode of Rayleigh and Love waves by a fully non-linear waveform inversion method (Yoshizawa and Kennett, 2002). In this method, the neighbourhood algorithm (Sambridge, 1999) is adopted as a global optimizer that explores the model space to find a model with the best fit to the recorded seismograms. Three thousand models were generated for each path and the best-fit 1-D model was obtained from among them. The multimode phase speeds were computed from the 1-D model using the normal mode theory (Takeuchi and Saito, 1972; Dahlen and Tromp, 1998), which are regarded as the path-averaged phase speeds of each event–station pair. The standard errors of each dispersion curve were estimated from the standard deviations of the best 1000 models among the ensemble of all the generated models. Here, we used the fundamental mode phase speeds of Rayleigh and Love waves. We used events with magnitude (Mb or Mw) greater than 5.7 for seismograms recorded at Japanese islands, where stations are densely located, and used events with magnitude (Mb or Mw) greater than 5.5 for oceanic island and BBOBS stations. The cross-correlation between observed and synthetic data with a group velocity filter, between 3.3 and 4.3 km/s for Rayleigh waves or between 3.3 and 4.7 km/s for Love

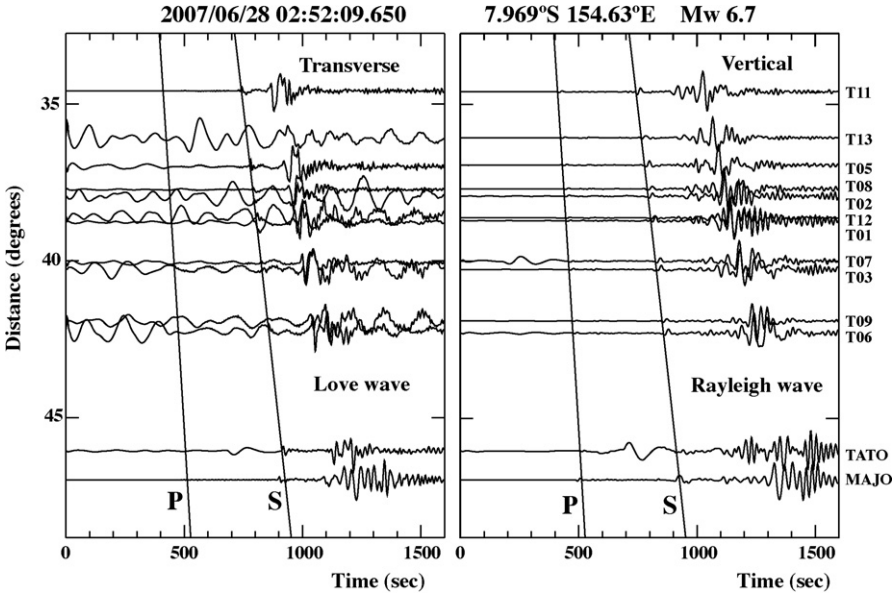

Fig. 2. Transverse and vertical components of a Solomon Islands event recorded at the BBOBS and island stations. Stations whose names starting with "T" are located on the seafloor and others (MAJO, TATO) are on island stations. Seismograms are filtered from 10 and 167 s and are plotted as displacement, with the instrumental response removed.

waves, is better than 0.9. We obtained 11,902 phase speed dispersion curves for Rayleigh waves and 8792 curves for Love waves at periods between 30 and 167 s.

To ensure uniform ray density, we clustered events observed at the same station with epicentres within a 100 km radius, and calculated the average phase speed for the group of events. We treated the average phase speed as the path-averaged phase speed along a ray from the centre of the cluster to the station. After clustering, we obtained 5555 path-averaged phase speed dispersion curves of Rayleigh waves, and 3480 of Love waves. The number of phase speed dispersion curves of Rayleigh and Love waves recorded by BBOBSs was 1241 and 158, respectively. The numbers of phase speed dispersion curves of Rayleigh waves recorded by all stations and OBS stations are 1.6 and 1.8 times higher, respectively, than those reported by Isse et al. (2009). The number of dispersion curves of Love waves recorded by BBOBSs is smaller than that of Rayleigh waves because the horizontal components of seismograms recorded by BBOBSs are noisier than the vertical components (Fig. 2).

2.3. Regionalization

Lateral phase-velocity variations are computed using the regionalization method developed by Montagner (1986). Following the approach of Smith and Dahlen (1973), the local azimuthally varying phase velocity $C(T, M, \Psi)$, at location M for each period T and azimuth Ψ, is expressed as follows:

$$C(T,M,\Psi) = C_{ref}(T)(1 + a_0(T,M) + a_1(T,M)\cos 2\Psi + a_2(T,M)\sin 2\Psi + a_3(T,M)\cos 4\Psi + a_4(T,M)\sin 4\Psi)$$

where C_{ref} is the reference model phase speed, the parameter a_0 is an isotropic term and a_i (i = 1–4) are the azimuthal anisotropy coefficients. The generalized least square inversion algorithm of Tarantola and Valette (1982) is used to regionalize the path-averaged phase speed of surface waves. In this paper, the covariance function (C_p) is defined as

$$C_p(M_1, M_2) = \sigma(M_1)\sigma(M_2)\exp\left[\frac{\cos\Delta - 1}{L^2}\right],$$

where Δ is the distance between points M_1 and M_2 on the Earth. The *a priori* parameter error σ_p gives a constraint on the anomaly amplitude and the correlation length L acts as a smoothing criterion.

Optimal values of the *a priori* parameter error and of correlation length are determined by a series of tests with synthetic data. We chose *a priori* parameter errors of 0.07 km/s for the isotropic parameter for both Rayleigh and Love waves and 0.04 km/s for the anisotropic parameter for Rayleigh waves. We selected a correlation length of 200 km for the isotropic parameters of Rayleigh and Love waves, and for the anisotropic parameters of Rayleigh waves. We used the average of path-averaged phase speeds as a reference phase speed. Montagner and Nataf (1986) demonstrated that the phase velocity of Rayleigh waves is mainly sensitive to azimuthal anisotropy through the 2Ψ terms, whereas the phase velocity of Love waves is mainly sensitive to the 4Ψ terms. Moreover, the 4Ψ coefficients are poorly resolved because of their rapid azimuthal variations. In the present study, we analyze the isotropic 0Ψ term of both surface waves and the 2Ψ terms of the phase velocity of Rayleigh waves.

2.4. Resolution tests

To assess the resolution of tomographic models and the correlation length, we first performed checkerboard resolution tests. We calculated the synthetic data from input checkerboard models with 6% isotropic anomalies at a period of 50 s: fast and slow anomalies of $4^\circ \times 4^\circ$ isotropic patterns for Rayleigh and Love waves, and $5^\circ \times 5^\circ$ anisotropic patterns with the fast azimuthal axis oriented N–S and E–W for Rayleigh waves (Fig. 3). The inversion was performed with the same correlation length (200 km for the 0Ψ and 2Ψ terms) and *a priori* errors as in the real case. We added random errors with amplitudes up to 0.5% to the synthetic data, which is the same as *a priori* errors in the real data. The $4^\circ \times 4^\circ$ isotropic patterns for Rayleigh waves are well reconstructed throughout the entire Philippine Sea plate, and the trade-off between isotropic phase speed and anisotropic parameters is less than 1.3% in the Philippine Sea region and 1.5% in the Pacific Ocean, (Fig. 3(a) and (b)). The $4^\circ \times 4^\circ$ isotropic patterns for Love waves are also well reconstructed for the entire Philippine Sea region (Fig. 3(c) and (d)). The anisotropic patterns for Rayleigh waves are well reconstructed only in the northern part of the Philippine Sea region, where the azimuthal coverage is good (Fig. 1(c)). The trade-off between anisotropic parameters and isotropic phase speed is less than 2.1% in the Pacific Ocean, and 1.8% in the northern Philippine Sea region.

The discrepancy in the recovered amplitudes of the phase velocities of Love and Rayleigh waves may produce artificial effects on the radial anisotropy (ξ) of shear waves. To address this problem, we assessed the recovered amplitudes of phase velocities of Love and Rayleigh waves in a checkerboard resolution test. The ray distribution is the same throughout the analyzed period range, indicating that the spatial resolutions are similar at periods between 30 and 167 s. This finding suggests that the ratio of the results of checkerboard synthetic tests of Rayleigh and Love waves can be used to assess the spatial resolution of ξ.

Fig. 4 shows the spatial distributions of the square of the ratios of Love wave phase speed to Rayleigh wave phase speed, $((C_L/C_{L0})/(C_R/C_{R0}))^2$. In the Philippine Sea region, $((C_L/C_{L0})/(C_R/C_{R0}))^2$ has values of 0.97–1.04. $((C_L/C_{L0})/(C_R/C_{R0}))^2$ is perturbed between values of 0.98 and 1.02 by the addition of 0.5% random errors to the synthetic data. These results suggest that there is no significant artificial pattern in the radial anisotropy caused by the discrepancy of recovered amplitudes of Love and Rayleigh waves in the Philippine Sea region. In the Pacific region, residuals of $((C_L/C_{L0})/(C_R/C_{R0}))^2$ are larger than those in the Philippine Sea region because the spatial resolution of the Love waves is worse than that of Rayleigh waves.

We have performed another synthetic test to assess the resolution of the likely structures in the analyzed region. Using the obtained maps of Rayleigh wave phase speed at periods of 50 and 100 s as input models, we calculated synthetic data, adding random errors up to 0.5%. We used only the isotropic part or anisotropic part of the obtained model as input models to assess the trade-off between isotropic and anisotropic structures.

Fig. 5 shows that the patterns of input models are well recovered at both periods and in both cases. The amplitudes of perturbations of isotropic patterns from average speeds at periods of 50 and 100 s in the Philippine Sea region are recovered at rates of about 65% and 60%, respectively (Fig. 5(b) and (e)). The amplitudes of anisotropic patterns for both periods are recovered at a rate of about 70% for the entire Philippine Sea region. The trade-off between isotropic and anisotropic patterns is less than 1.4% and 1.1% at periods of 50 and 100 s, respectively. The azimuthal difference between the input and output models is less than 15° for the entire Philippine Sea region. The trade-off between isotropic and anisotropic parameters is less than 1.6% for both periods. The trade-offs are much smaller than the recovered models, indicating that the features in our models are real and robust. The findings of this synthetic test suggest that the patterns of obtained isotropic and anisotropic structures are well recovered and that their amplitudes are recovered at a rate of about 65% throughout the entire Philippine Sea.

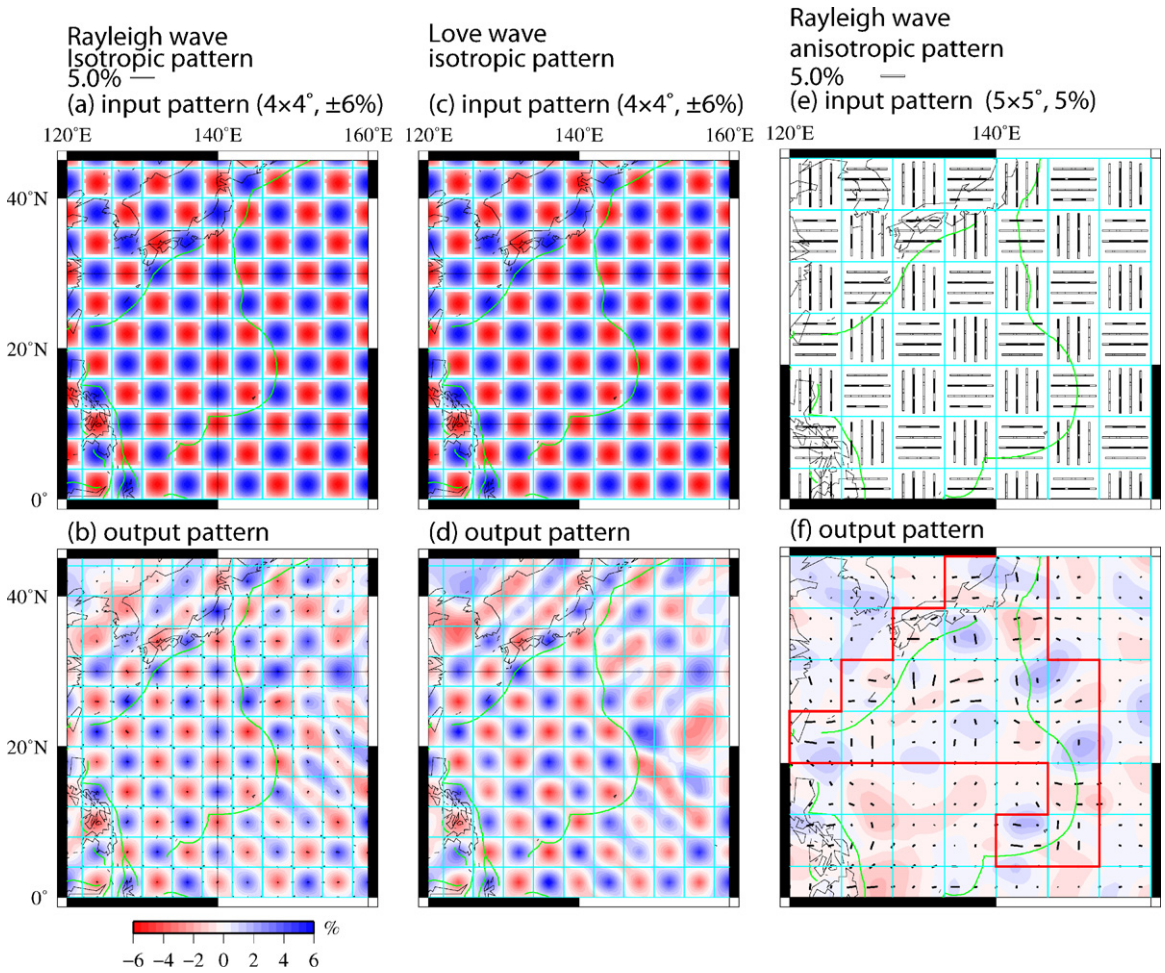

Fig. 3. Checkerboard resolution tests for Rayleigh and Love waves at 50 s. (a) $4^\circ \times 4^\circ$ isotropic patterns with 6% anomalies for Rayleigh waves. (b) Output patterns of (a). (c) $4^\circ \times 4^\circ$ isotropic patterns with 6% anomalies for Love waves. (d) Output of (c). The patterns are well recovered in the Philippine Sea region. (e) $5^\circ \times 5^\circ$ anisotropic patterns with 5% anomalies for Rayleigh waves. Black lines in (e) show the anisotropies in the same locations as the output patterns. (f) Output pattern of (e). The area enclosed by red lines is a well-resolved area. (For interpretation of the references to color in this figure legend, the reader is referred to the web version of the article.)

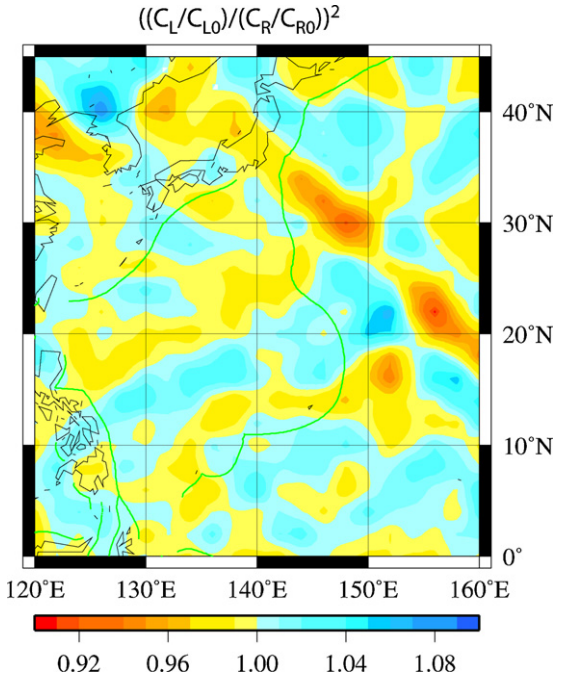

Fig. 4. $((C_L/C_{L0})/(C_R/C_{R0}))^2$ calculated based on the results of isotropic patterns of Rayleigh and Love waves shown in Fig. 3(b) and (d).

The results of the above synthetic tests suggest that the patterns of azimuthal anisotropy are well resolved in the northern Philippine Sea region with a lateral resolution of 500 km, and radial anisotropy (derived from the discrepancy between Rayleigh and Love waves) appears throughout the entire Philippine Sea region with a lateral resolution of 400 km. In the southern Philippine Sea, the test results suggest that the obtained azimuthal anisotropy is well recovered and that the lateral resolution is much larger than 500 km.

2.5. S-wave velocity inversion

Following Montagner and Nataf (1986), 13 parameters are required to explain surface wave data (Rayleigh and Love waves) in the most general case for weak anisotropy. Using their notation, the Rayleigh wave phase-velocity dispersion $\delta C_R(T, M, \Psi)$ is expressed as

$$\delta C_R(T, M, \Psi) = \frac{\partial C_R}{\partial A}(\delta A + B_C \cos 2\Psi + B_S \sin 2\Psi + E_C \cos 4\Psi + E_S \sin 4\Psi) + \frac{\partial C_R}{\partial C}\delta C + \frac{\partial C_R}{\partial F}(\delta F + H_C \cos 2\Psi + H_S \sin 2\Psi) + \frac{\partial C_R}{\partial L}(\delta L + G_C \cos 2\Psi + G_S \sin 2\Psi).$$

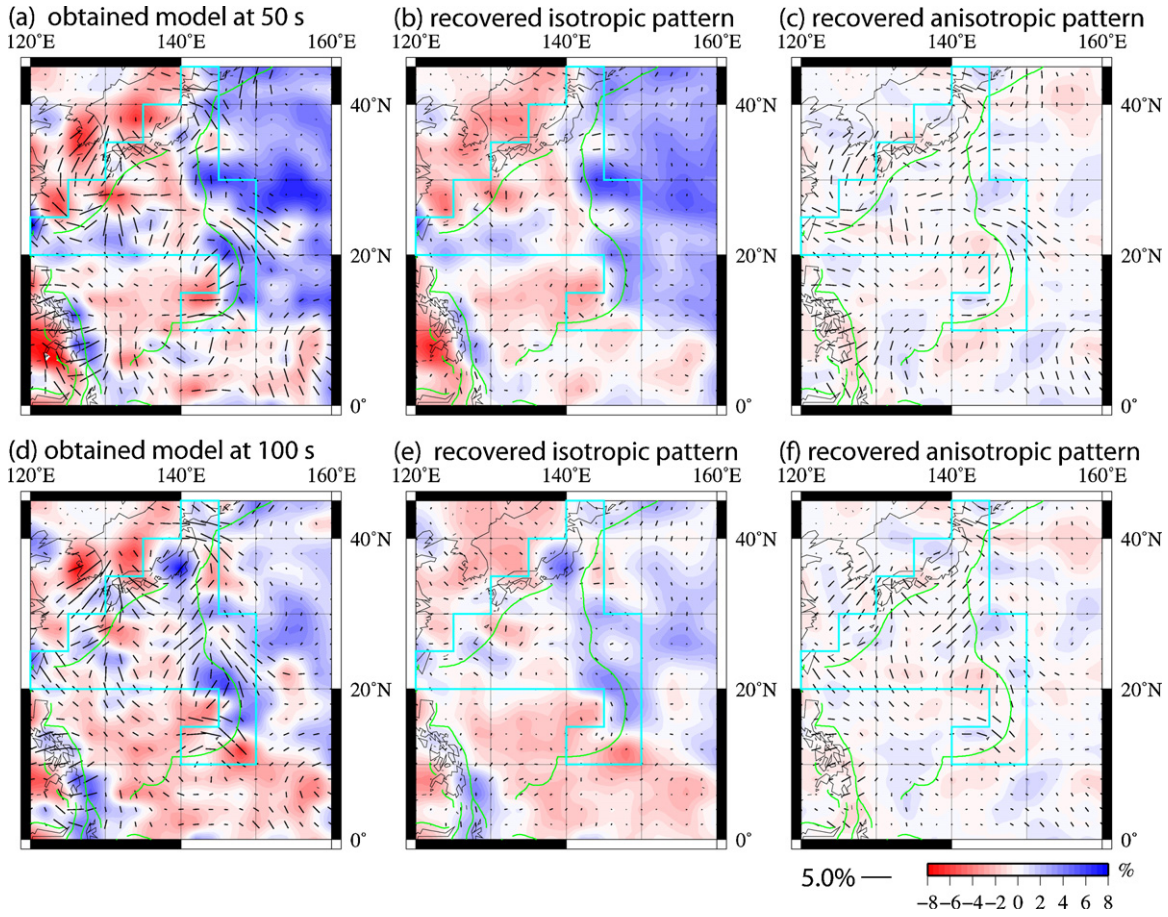

Fig. 5. Synthetic tests using the obtained phase-velocity maps at periods of 50 and 100 s. (a and d) Obtained Rayleigh wave phase-velocity maps at periods of 50 and 100 s, respectively. (b and e) Output results calculated from isotropic patterns in (a and d), respectively. The isotropic patterns are well recovered and the trade-off to anisotropic patterns are less than 1.6%, 1.1% at periods of 50 and 100 s, respectively. (c and f) Output results calculated from anisotropic patterns in (a and d), respectively. The anisotropic patterns are well recovered and the trade-off to isotropic patterns are less than 1.6%.

Similarly, for Love wave phase-velocity perturbations, $\delta C_L(T, M, \Psi)$ is

$$\delta C_L(T, M, \Psi) = \frac{\partial C_L}{\partial L}(\delta L - G_C \cos 2\Psi - G_S \sin 2\Psi) + \frac{\partial C_L}{\partial N}(\delta N - E_C \cos 4\Psi - E_S \sin 4\Psi).$$

The kernels $\partial C_{R,L}/\partial p_i$ are calculated in the spherically symmetric reference model based on anisotropic PREM model (Dziewonski and Anderson, 1981), except for the crust for which we adopted the CRUST 2.0 model (Bassin et al., 2000). The inverse problem is resolved using a non-linear least squares inversion algorithm (Tarantola and Valette, 1982). The errors in phase velocities obtained from the regionalization procedure are taken into account, and the final error in the parameters is estimated by computing the *a posteriori* covariance matrix. The model is described by 20-km-thick layers and a Gaussian correlation between adjacent layers is introduced. The inversion is performed using the 13 parameters per layer, but only 4 parameters are well resolved: L, N, G_C and G_S. Therefore, only the following parameters of the 3-D model are presented as a function of depth:

$$V_{SV} = \sqrt{\frac{L + G_c \cos 2\Psi + G_S \sin 2\Psi}{\rho}}, \quad \xi = \left(\frac{V_{SH}}{V_{SV}}\right)^2 = \frac{N}{L},$$

where V_{SV} and V_{SH} are the vertically and horizontally polarized S-wave velocity, respectively.

3. Results

3.1. Shear-wave velocity structures in the Philippine Sea region

The result of the resolution tests suggests that the northern part of the Philippine Sea region, where dense seafloor observations have been deployed, is well resolved. Fig. 6 shows the 3-D shear-wave velocity structures (isotropic shear-wave speed anomalies (ΔV_{SV}), SV wave azimuthal anisotropy (G), and radial anisotropy (ξ)) beneath the northern Philippine Sea region at depths of 58, 100, 140, and 180 km. At a depth of 58 km, three slow isotropic anomalies appear along the Izu–Ogasawara–Mariana island arc and isotropic fast anomalies are seen in the West Philippine Basin and Pacific Ocean. At depths greater than 100 km, the subducting Pacific plate can be seen along the Izu–Ogasawara–Mariana subduction zone. These isotropic anomalies are consistent with those evident in our previous model (Isse et al., 2009).

The azimuthal variation of the fast direction of the anisotropic parameter G at depths shallower than 140 km is different from that at depths greater than 140 km (Fig. 6(a), (c), (e) and (g)). In the shallow part, the fast directions of azimuthal anisotropy in the Shikoku Basin are E–W and those in the Pacific Ocean are NW–SE (Fig. 6(a) and (c)). In the deep part, the fast directions of the azimuthal anisotropy beneath the Shikoku Basin are WNW–ESE, those beneath the Izu–Ogasawara island arc are NE–SW, those beneath the Philippine Sea are NW–SE, and those beneath the Guam Island vary from E–W to NW–SE. A large-scale pattern of NW–SE fast directions is seen in the southern Philippine Sea region.

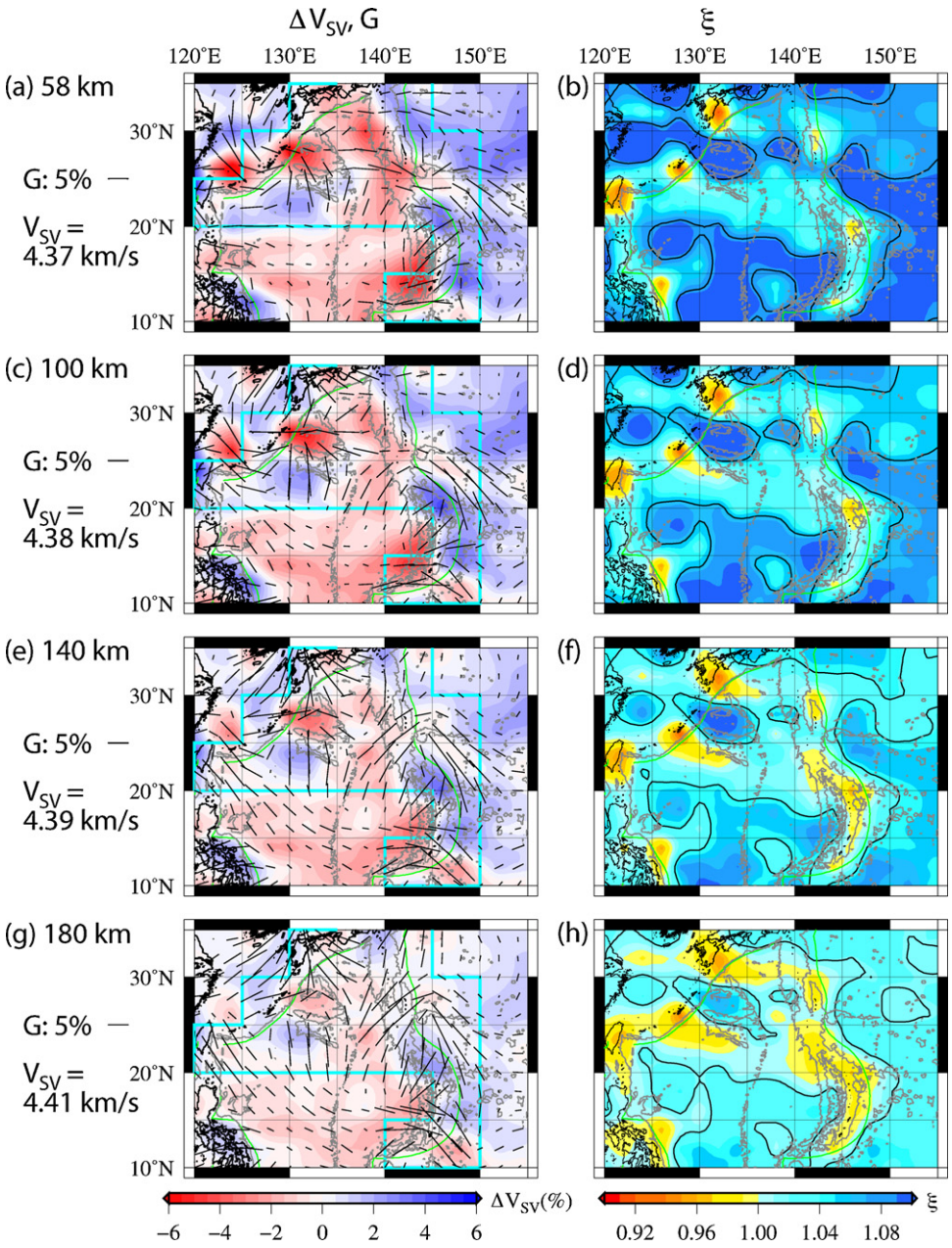

Fig. 6. Map projections of the isotropic shear-wave perturbations (ΔV_{SV}), fast direction, and amplitude of azimuthal anisotropy(G) (a, c, e and g), and radial anisotropy (ξ) (b, d, f and h) at depths of (a and b) 58, (c and d) 100, (e and f) 140, and (g and h) 180 km. The area surrounded by light blue lines in (a, c, e and f) is a well-resolved area in the case of azimuthal anisotropy. The black lines in (a, c, e and f) show the fast directions and amplitude of the azimuthal anisotropy. The black lines in (b, d, f and h) show the radial anisotropy (ξ) in the anisotropic PREM model.

Fig. 6(b), (d), (f) and (h) shows the radial anisotropy (ξ). The shear-wave structures in PREM at depths between 24.4 and 220 km have radial anisotropy with positive ξ. Areas of weak radial anisotropy (compared to anisotropic PREM), marked by light blue and yellow areas within solid black lines in Fig. 6(b), (d), (f) and (h), occur around the margin and in the central part of the Philippine Sea plate. Fast V_{SV} structures and $\xi < 1.0$ are seen at the margin of the Philippine Sea plate, the Izu–Ogasawara island arc and the Philippines (Fig. 6). These findings indicate near-vertical downwelling (i.e., downward vertical flow) in the Pacific and Philippine subduction zone. The strong lateral variation of the radial anisotropy is different from that seen in the Pacific plate, which has a strong radial anisotropy. In the Pacific plate, radial anisotropy is strongest in the central part of the plate (Ekström and Dziewonski, 1998).

The above results suggest that radial anisotropy is not especially strong in the centre of the Philippine Sea plate and that its average amplitude is smaller than that of PREM. The lateral variations of radial anisotropy are similar at all depths analyzed in this study, although the isotropic variations vary with depth.

4. Discussion

4.1. Lithosphere and asthenosphere in the Philippine Sea region

In the oceanic lithosphere, the fast axis of the seismic velocity (associated with olivine LPO) is subhorizontal and aligned approximately parallel to the direction of ancient seafloor spreading (Nicolas and Christensen, 1987). In the asthenosphere, the fast axis is explained by the alignment of olivine *a*-axes parallel to

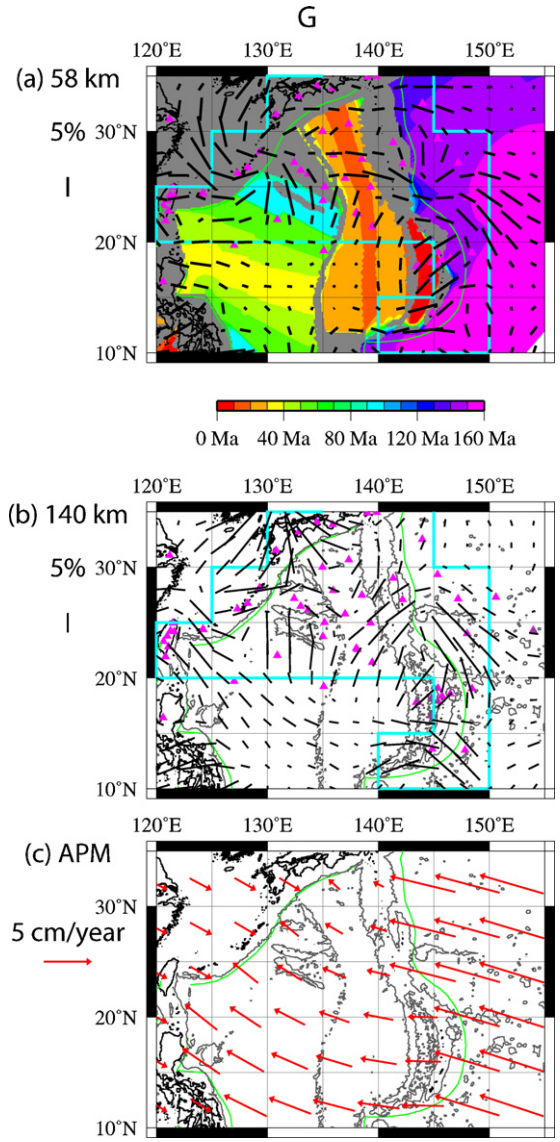

Fig. 7. Map projections of azimuthal anisotropy at depths of (a) 58 km with isochrones and (b) 140 km. The present-day absolute plate motions (APM), as derived from NNR-NUVEL1A, are shown in (c). Green lines represent plate boundary. Light blue lines in (a and b) are well-resolved area in the case of azimuthal anisotropy. (For interpretation of the references to color in this figure legend, the reader is referred to the web version of the article.)

present-day flow. Many previous studies analyzed the anisotropic structures of shear waves on a global scale (e.g., Montagner and Tanimoto, 1991; Debayle et al., 2005) or semi-global scale (Montagner and Jobert, 1988; Nishimura and Forsyth, 1989). However, no previous study has investigated a back-arc basin with a range of seafloor ages and tectonic features.

Fig. 7(a) and (b) shows the azimuthal anisotropy in the Philippine Sea region at depths of 58 and 140 km. The seafloor ages from Müller et al. (2008) are superimposed on Fig. 7(a). Fig. 7(c) shows the present-day absolute plate motion (APM) from NNR-NUVEL1A (DeMets et al., 1994). The thickness of the oceanic lithosphere is about 40–120 km based on half-space cooling model with seafloor ages of 20–160 Ma (Parker and Oldenburg, 1973); consequently, Fig. 7(a) shows anisotropic structures in the lithosphere, while Fig. 7(b) shows those in the asthenosphere.

In the Shikoku Basin, the northern part of the West Philippine Basin and the Pacific Ocean, the fast velocity axes at a depth of 58 km are approximately perpendicular to the isochrons; i.e., sub-parallel to the direction of ancient seafloor spreading (Fig. 7(a)). This result suggests that fossil alignment of the crystallographic axes of olivine in the lithosphere occurs not only in large oceanic plates such as the Pacific plate but also in back-arc basins such as the Shikoku and West Philippine Basins. In the northern part of the Parece-Vela Basin, the fast velocity axes are not oriented perpendicular to the isochrons. In the Mariana Trough, the direction of the fast axes is parallel or oblique to the isochrons. This region was poorly resolved because the Mariana Trough is smaller than the spatial resolution of our azimuthal anisotropy model (~500 km).

In the Pacific Ocean, the fast axes of azimuthal anisotropy at a depth of 140 km are oriented about 30° from the direction of the APM of the Pacific plate (Fig. 7(b) and (c)), being parallel to the direction of ancient seafloor spreading. The fast axes of azimuthal anisotropy in the Shikoku Basin are oriented sub-parallel to those in the Philippine Sea plate. In the northern part of the West Philippine Basin, the fast axes are oblique to the direction of the APM of the Philippine Sea plate (by about 55°).

4.2. Nature of the Philippine Sea plate

The Philippine Sea plate is regarded as a single plate, primarily because of a lack of intraplate seismicity. However, the azimuthal and radial anisotropies within this plate show strong lateral variations. This is in contrast with the Pacific plate, which shows a relatively uniform distribution of azimuthal anisotropy in good agreement with the theory of plate tectonics except around hotspots (Montagner, 2002), and a strong radial anisotropy in the centre of the plate (Ekström and Dziewonski, 1998).

The observed lateral variations in azimuthal anisotropy within the lithosphere of the northern part of the Philippine Sea plate at a depth of 58 km show a strong correlation with the ancient seafloor spreading. The variation at depths greater than 140 km suggests a large-scale flow from the Guam Island, toward the southern part of the Philippine Sea plate with E–W direction of azimuthal anisotropy, followed by coherent flow northward to The Philippines, and Taiwan. At Guam, the flow direction changes from NW–SE to E–W. Although the checkerboard test with a $5^\circ \times 5^\circ$ pattern shows this region as a relatively poorly resolved area (Fig. 3(f)), the size of the flow exceeds $5^\circ \times 5^\circ$ and the results of another synthetic test performed using our result as an input model suggested that the patterns have been recovered and that there exists only a small trade-off between isotropic and anisotropic patterns (Fig. 5(d)–(f); consequently, this large-scale flow is considered to be a real feature. One explanation of this change in flow direction is that NW–SE mantle flow in the Pacific encounters the subducting Pacific plate at Guam, forcing a change in flow direction to E–W. Along the Izu–Ogasawara island arc, the fast axis of azimuthal anisotropy is oriented NE–SW at a depth of 140 km, in contrast to the present APM of the Philippine Sea plate and Pacific plates. We consider that these directions (NE–SW) are caused by the anisotropy in the subducting Pacific plate.

4.3. Detailed structures within the northern part of the Philippine Sea plate

To analyze the detailed structure of the lithosphere and asthenosphere in the northern Philippine Sea plate, we constructed the depth profiles of isotropic variation of the shear-wave speed (V_{SV}), azimuthal anisotropy (ΔG), and radial anisotropy (ξ) in the Shikoku Basin, West Philippine Basin, and northwestern Pacific Ocean (Fig. 8(a)–(c)). Plomerová et al. (2002) used this approach to map changes in the patterns of anisotropy in order to estimate the depth of the lithosphere–asthenosphere boundary. Instead of showing the average profiles for each region, we show data for a single point because the structure of the asthenosphere varys in the region where the structure of the lithosphere is similar.

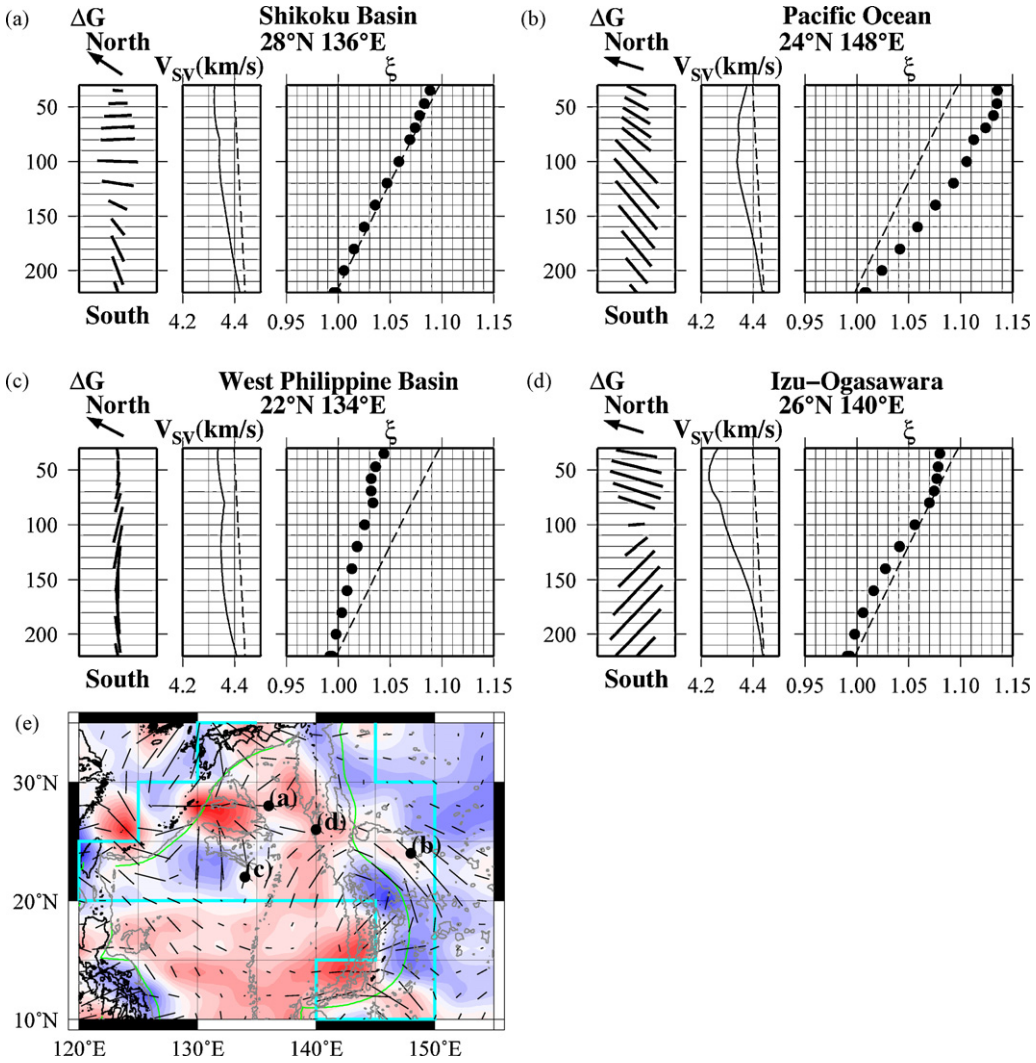

Fig. 8. Depth profiles of azimuthal anisotropy (ΔG), shear-wave speed (V_{SV}), and radial anisotropy (ξ) in (a) the Shikoku Basin, (b) the Pacific Ocean, (c) the northern part of the West Philippine Basin, and (d) the Izu–Ogasawara island arc. North of azimuthal anisotropy (ΔG) is oriented in a shallower depth direction (upwards). Broken line in V_{SV} indicates the V_{SV} of the PREM model. Broken lines in ξ indicate the amplitude of the anisotropic PREM model. (e) V_{SV} and G structures at a depth of 100 km, as shown in Fig. 6(c); also shown are the locations of (a–d). The arrow in the upper part of ΔG indicates the APM in each location.

In the Shikoku Basin, V_{SV} is slowest at a depth of 60 km, and ξ is similar to that in the PREM model. The fast direction of azimuthal anisotropy is approximately E–W, which is sub-parallel to the direction of ancient seafloor spreading at depths shallower than 100 km; at greater depth, it becomes parallel to the APM direction.

In the Pacific Ocean, V_{SV} is slowest at a depth of 100 km and ξ is larger than that in the PREM model. The fast direction is constantly NW–SE, although the amplitude is greatest at a depth of 100 km. The direction is similar to the direction of the ancient seafloor spreading. In this region, the difference between the direction of ancient seafloor spreading and the APM direction is about 30°; consequently, it is difficult to detect the depth of the azimuthal change of ΔG.

In the West Philippine Basin, V_{SV} is fastest at a depth of 80 km. The fast direction of the azimuthal anisotropy is N–S, sub-parallel to the direction of ancient seafloor spreading at depths shallower than 100 km, and is also N–S at greater depth. The APM direction is approximately NW–SE in this region, meaning that the fast direction of the azimuthal anisotropy is oblique to the APM direction by about 60°. The depth profile is very different from that obtained for the other two regions. The value of ξ is large up to 80 km depth, but decreases with depth thereafter.

Using a similar approach to that adopted by Plomerová et al. (2002), we estimate the thickness of the lithosphere based on the changes in anisotropy. The isotropic and anisotropic structures suggest that the lithosphere thickness is about 60, and 100 km in the Shikoku Basin, and Pacific Ocean, respectively. The low V_{SV} values may indicate the lithosphere–asthenosphere boundary in the Shikoku Basin and the Pacific Ocean. We could not estimate the lithosphere thickness in the West Philippine Basin, because there is no significant change of low V_{SV} values and the azimuth of ΔG in depth. V_{SH} is faster than V_{SV} in these three regions; however, the depth variation of ξ in the West Philippine Basin is different from that in the Shikoku Basin and the Pacific Ocean, where the gradient in ξ is similar to that in the PREM model. ξ in the West Philippine Basin is smaller than that in the PREM model. Because the V_{SV} structures suggest a thick lithosphere, one possible explanation of the small ξ is that old ridges (i.e., the Amami Plateau, Daito ridge, and Oki-Daito ridge), which have thick crust, have an effect on the radial anisotropy.

4.4. Azimuthal anisotropy around the subduction zone

In the Mariana Trough at depths shallower than 100 km, the fast direction of the azimuthal anisotropy is NE–SW; at greater

depths, it is N–S in the northern part of the trough and E–W in the southern part. In the northern part, the fast direction shows trench-parallel anisotropy. These features are consistent with the result reported by Pozgay et al. (2007) based on shear-wave splitting measurements of local S-waves recorded by a temporary observation network consisting of OBS and island stations in and around the Mariana arc. The E–W fast direction in the southern part of the Mariana Trough is also consistent with the result of previous studies based on an analysis of shear-wave splitting around the Guam (Fouch and Fischer, 1998; Volti et al., 2006).

In the Izu–Ogasawara island arc, the fast direction at a depths of 140 and 180 km is NE–SW, which is highly different to that in the surrounding area (Fig. 6(e) and (g)). This difference may be due in part to the subducting Pacific plate. To analyze the detailed structures of the anisotropy, we constructed a depth profile of the isotropic and anisotropic variations (Fig. 8(d)). The amplitude of azimuthal anisotropy is smallest at a depth of 100 km, and the fast direction shows a rapid change at this depth. At depths less than 100 km, the fast direction is WNW–ESE; at greater depths it is NE–SW. The observed radial anisotropy suggests that V_{SV} is faster than V_{SH} at depths greater than 180 km. The top of the subducting Pacific plate lies at a depth of 150 km; consequently, these features are characteristic of the subducting Pacific plate itself.

In the Ryukyu arc, the fast direction of azimuthal anisotropy is NW–SE at a depth of 58 km (Fig. 6(a)), and is parallel to the trench at depths deeper than 80 km. Long and van der Hilst (2006) reported trench-parallel anisotropy in the mantle wedge below the Ryukyu arc based on measurements of shear-wave splitting from local slab earthquakes recorded at seismic stations within the arc. The present results are consistent with those of these earlier results.

The above results suggest the existence of various types of azimuthal anisotropy around the subduction zones in the Philippine Sea plate, possibly caused by the complex pattern of the subduction system.

5. Conclusions

We analyzed the isotropic and anisotropic shear-wave velocity structures in the northern Philippine Sea region using Rayleigh and Love waves recorded by land and seafloor observations. We found that the fast directions of azimuthal anisotropies are oriented parallel to the direction of ancient seafloor spreading in the lithosphere of the Shikoku and West Philippine Basins and Pacific Ocean, parallel to the direction of the present-day APM in the asthenosphere of the Shikoku Basin, and oblique to the direction of the APM in the Pacific Ocean (by about 30°) and in the northern part of the West Philippine Basin (by about 55°). In the subduction zones at the margin of the Philippine Sea plate, the fast direction of azimuthal anisotropy is parallel to the trench in the Ryukyu arc, and NW–SE directions in the Izu–Ogasawara island arc.

Acknowledgments

We thank the staff of the IRIS, OHP, SPANET and the F-net data centre for their efforts in maintaining and managing the seismic stations. We also thank the officers and crew of the R/V Kairei (JAMSTEC) and Asean Maru (Dokai Marine Systems, Ltd.) for their reliable work and efficient support during the cruises. We also thank two anonymous reviewers fort their helpful comments. This work was supported by a Grant-in-Aid for Scientific Research [KAKENHI, 16075203] from the Japan Society for the Promotion Science. This study made use of the GMT software package (Wessel and Smith, 1991) and SAC2000 (Goldstein and Minner, 1996).

References

Aki, K., Kaminuma, K., 1963. Phase velocity in Japan. Part I. Love waves from the Aleutian shocks of March 9, 1957. Bull. Earthq. Res. Inst. 41, 243–259.
Bassin, C., Laske, G., Masters, G., 2000. The current limits of resolution for surface wave tomography in North America. Eos Trans. AGU Fall Meet. Suppl. 81, Abstract: S12A-03.
Debayle, E., Kennett, B., Priestley, K., 2005. Global azimuthal seismic anisotropy and the unique plate-motion deformation of Australia. Nature 433, 509–512.
DeMets, C., Gordon, R.G., Argus, D.F., Stein, S., 1994. Effect of recent revisions to the geomagnetic reversal time scale on estimates of current plate motions. Geophys. Res. Lett. 21, 2191–2194.
Dahlen, F., Tromp, J., 1998. Theoretical Global Seismology. Princeton Univ. Press, Princeton, NJ.
Dziewonski, A.M., Anderson, D.L., 1981. Preliminary reference Earth model. Phys. Earth Planet. Inter. 25, 297–356.
Ekström, G., Dziewonski, A.M., 1998. The unique anisotropy of the Pacific upper mantle. Nature 394, 168–172.
Forsyth, D.W., 1975. The early structural evolution and anisotropy of the oceanic upper mantle. Geophys. J. R. Astr. Soc. 43, 103–162.
Fouch, M.J., Fischer, K.M., 1998. Shear wave anisotropy in the Mariana subduction zone. Geophys. Res. Lett. 25, 1221–1224.
Goldstein, P., Minner, L., 1996. SAC2000: seismic signal processing and analysis tools for the 21st century. Seismol. Res. Lett. 67, 39.
Gorbatov, A., Kennett, B.L.N., 2003. Joint bulk-sound and shear tomography for Western Pacific subduction zones. Earth Planet. Sci. Lett. 210, 527–543.
Hall, R., Ali, J.R., Anderson, C.D., Baker, S.J., 1995. Origin and motion history of the Philippine Sea plate. Tectonophysics 251, 229–250.
Hess, H.H., 1964. Seismic anisotropy of the uppermost mantle under oceans. Nature 203, 629–631.
Hussong, D.M., Uyeda, S., 1981. Tectonic processes and the history of the Mariana arc: a synthesis of the results of deep sea drilling project leg 60. Initial Rep. Deep Sea Drill. Proj. 60, 909–929.
Isse, T., Yoshizawa, K., Shiobara, H., Shinohara, M., Nakahigashi, K., Mochizuki, K., Sugioka, H., Suetsugu, D., Oki, S., Kanazawa, T., Suyehiro, K., Fukao, Y., 2006. Three-dimensional shear wave structure beneath the Philippine Sea from land and ocean bottom broadband seismograms. J. Geophys. Res. 111, B06310, doi:06310.01029/02005JB003750.
Isse, T., Shiobara, H., Tamura, Y., Suetsugu, D., Yoshizawa, K., Sugioka, H., Ito, A., Kanazawa, T., Shinohara, M., Mochizuki, K., Araki, E., Nakahigashi, K., Kawakatsu, H., Shito, A., Fukao, Y., Ishizuka, O., Gill, J.B., 2009. Seismic structure of the upper mantle beneath the Philippine Sea from seafloor and land observation: Implications for mantle convection and magma genesis in the Izu–Bonin–Mariana subduction zone. Earth Planet. Sci. Lett. 278, 107–119.
Kanamori, H., Abe, K., 1968. Deep structure of island arcs as revealed by surface waves. Bull. Earthq. Res. Inst. 46, 1001–1025.
Kanazawa, T., Shiobara, H., Mochizuki, M., Shinohara, M., Araki, E., 2001. Seismic observation system on the sea floor. In: Proceedings of OHP/ION Joint Symposium, Long-Term Observations in the Oceans. Earthq. Res. Inst., Univ. of Tokyo, S11–16.
Kawakatsu, H., Kumar, P., Takei, Y., Shinohara, M., Kanazawa, T., Araki, E., Suyehiro, K., 2009. Seismic evidence for sharp lithosphere–asthenosphere boundaries of oceanic plates. Science 324, 499–502.
Lebedev, S., Nolet, G., van der Hilst, R.D., 1997. The upper mantle beneath the Philippine Sea region from waveform inversions. Geophys. Res. Lett. 24, 1851–1854.
Long, M.D., van der Hilst, R.D., 2006. Shear wave splitting from local events beneath the Ryukyu arc: trench-parallel anisotropy in the mantle wedge. Phys. Earth Planet. Inter. 155, 300–312.
Montagner, J.-P., 1986. Regional three-dimensional structures using long-period surface waves. Ann. Geophys. 4, 283–294.
Montagner, J.-P., 2002. Upper mantle low anisotropy channels below the pacific plate. Earth Planet. Sci. Lett. 202, 263–274.
Montagner, J.-P., Jobert, N., 1988. Vectorial tomography. II. Application to the Indian Ocean. Geophys. J. R. Astr. Soc. 94, 309–344.
Montagner, J.-P., Nataf, H., 1986. A simple method for inverting the azimuthal anisotropy of surface waves. J. Geophys. Res. 91, 511–520.
Montagner, J.-P., Tanimoto, T., 1991. Global upper mantle tomography of seismic velocities and anisotropies. J. Geophys. Res. 96, 20337–20351.
Müller, R.D., Sdrolias, M., Gaina, C., Roest, W.R., 2008. Age, spreading rates, and spreading asymmetry of the world's ocean crust. Geochem. Geophys. Geosyst. 9, Q04006, doi:10.1029/2007GC001743.
Nakamura, Y., Shibutani, T., 1998. Three-dimensional shear wave velocity structure in the upper mantle beneath the Philippine Sea region. Earth Planets Space 50, 939–952.
Nicolas, A., Christensen, N.I., 1987. Formation of anisotropy in upper mantle peridotites – a review. In: Froidevaux, C., Fuchs, K. (Eds.), The Composition, Structure and Dynamics of the Lithosphere–Asthenosphere System, vol. 16. AGU Geophys. Ser. AUG, Washington, DC, pp. 111–123.
Nishimura, C.E., Forsyth, D.W., 1989. The anisotropic structure of the upper mantle in the Pacific. Geophys. J. 96, 203–229.
Oda, H., Senna, N., 1994. Regional variation in surface wave group velocities in the Philippine Sea. Tectonophysics 233, 265–277.
Okino, K., Ohara, Y., Kasuga, S., Kato, Y., 1999. The Philippine Sea: new survey results reveal the structure and the history of the marginal basins. Geophys. Res. Lett. 26, 2287–2290.

Parker, R.L., Oldenburg, D.W., 1973. Thermal model of ocean ridges. Nat. Phys. Sci. 242, 137–139.
Plomerová, J., Kouba, D., Babuška, V., 2002. Mapping the lithosphere–asthenosphere boundary through changes in surface-wave anisotropy. Tectonophysics 358, 175–185.
Pozgay, S.H., Wiens, D.A., Conder, J.A., Shiobara, H., Sugioka, H., 2007. Complex mantle flow in the Mariana subduction system: evidence from shear wave splitting. Geophys. J. Int. 170, 371–386.
Sambridge, M., 1999. Geophysical inversion with a neighbourhood algorithm. I. Searching a parameter space. Geophys. J. Int. 138, 479–494.
Shiobara, H., Kato, M., Sugioka, H., Yoneshima, S., Mochizuki, M., Mochizuki, S., Kodaira, S., Hino, R., Shinohara, M., Kanazawa, T., 2001. Long term observation by ocean bottom seismometer array on trans-PHS profile. In: Proceedings of OHP/ION Joint Symposium, Long-Term Observations in the Oceans. Earthquake Res. Inst., Univ. of Tokyo, S11–10.
Shiobara, H., Baba, K., Utada, H., Fukao, Y., 2009. Ocean bottom array probes stagnant slab beneath the Philippine Sea. Eos Trans. AGU 90, 70–71.
Smith, M., Dahlen, F., 1973. The azimuthal dependence of Love and Rayleigh wave propagation in a slightly anisotropic medium. J. Geophys. Res. 78, 3321–3333.
Takeuchi, H., Saito, M., 1972. Seismic surface waves. In: Bolt, E.A. (Ed.), Seismology: Surface Waves and Free Oscillations, Methods. Comput. Phys., vol. 11. Academic, pp. 217–295.
Tarantola, A., Valette, B., 1982. Generalized nonlinear inverse problems solved using the least squares criterion. Rev. Geophys. Space Phys. 20, 219–232.
Taylor, B., Goodliffe, A.M., 2004. The West Philippine Basin and the initiation of subduction, revisited. Geophys. Res. Lett. 31, doi:10.1029/2004GL020136.
Vinnik, L., Farra, V., Romanowicz, B., 1989. Azimuthal anisotropy in the earth from observations of SKS at Geoscope and Nars broad band stations. Bull. Seism. Soc. Am. 79, 1542–1558.
Volti, T., Gorbatov, A., Shiobara, H., Sugioka, H., Mochizuki, K., Kaneda, Y., 2006. Shear-wave splitting in the Mariana trough – a relation between back-arc spreading and mantle flow? Earth Planet. Sci. Lett. 244, 566–575.
Wessel, P., Smith, W.H.F., 1991. Free software helps map and display data. Eos Trans. AGU 72, 441, 445–446.
Yoshizawa, K., Kennett, B.L.N., 2002. Non-linear waveform inversion for surface waves with a neighbourhood algorithm – application to multimode dispersion measurements. Geophys. J. Int. 149, 118–133.